J. Micromech. Microeng. **21** (2011) 045009 (12pp) doi:10.1088/0960-1317/21/4/045009

Analysis of nanoscale mechanical grasping under ambient conditions

Hui Xie[1], **Pierre Lambert**[2] **and Stéphane Régnier**[1]

[1] Institut des Systèmes Intelligents et Robotique, Université Pierre et Marie Curie/CNRS UMR7222 BC 173, 4 Place Jussieu, 75005 Paris, France
[2] BEAMS Department, Université libre de Bruxelles, CP 165/56, 50 Avenue FD Roosevelt, B-1050 Bruxelles, Belgium

E-mail: xie@isir.upmc.fr

Received 11 October 2010, in final form 16 December 2010
Published 4 March 2011
Online at stacks.iop.org/JMM/21/045009

Abstract
In this paper, in order to understand mechanical grasping at the nanoscale, contact mechanics between nanogrippers and nanoobjects is studied. Contact models are introduced to simulate elastic contacts between various profiles of a flat surface, sphere and cylinder for different types of nanoobjects and nanogrippers. Analyses and evaluation instances indicate that friction forces, commonly used in macro-grasping to overcome gravity, at the nanoscale are often insufficient to overcome the relatively strong adhesion forces when picking up the nanoobject deposited on a substrate due to the tiny contact area. For stable nanoscale grasping, nonparallel two-finger grippers with a 'V' configuration are demonstrated to have better grasping capabilities than parallel grippers. To achieve mechanical nanoscale grasping, a nanogripper constructed from two microcantilevers is presented. Experimental results for the pick-and-place manipulation of silicon nanowires validate the theoretical analyses and capabilities of the proposed nanogripper.

(Some figures in this article are in colour only in the electronic version)

1. Introduction

Grasping has been widely used to move an object from one place to another for macro-mechanical manipulation and assembly. Research efforts have been made to scale mechanical grasping down to the microscale with microgrippers to integrate functional micro components into mechatronics systems or to perform scientific explorations in biology [1–6]. Recent work has reported that pick-and-place manipulation at the scale of several micrometers has been achieved with a dual-probe gripper [7]. Some basic micromanipulation problems attributed to the scale effects [8], such as suitable grasping principles and release techniques taking adhesion forces into account, have been identified. However, the scale effects become more severe at the nanoscale. In this case, the very tiny size of a nanoobject to be grasped generates higher requirements for grasping schemes and nanogripper fabricating techniques.

In the past two decades, nanomanipulation has usually been restricted to building 2D nanopatterns or in-plane nanomaterial characterization through pushing or pulling manipulation on a single surface with atomic force microscopes (AFM) [9–12]. Nanostructures have, however, been manipulated, assembled and characterized by nanorobots equipped with manipulators or grippers in scanning electron microscopes (SEM) or transmission electron microscopes (TEM) [13–15], in which nanoscale grasping can be performed due to the vacuum environment and the visual feedback. A liquid medium enables noncontact nanoscale grasping where the adhesion forces are greatly reduced, e.g., optical tweezer [16]. In order to fabricate smart nanogrippers, carbon nanotube (CNT) materials have been used as self-actuated gripper fingers [17]. However, the alignment of CNT fingers remains a challenge, and the grasping capabilities of the CNT nanotweezer still need further testing and verification, especially for grasping under ambient conditions with the presence of strong adhesion forces.

To achieve mechanical nanoscale grasping, the main difficulties are fabricating very sharp end-effectors with a size comparable to the nanoobject to be manipulated and with

enough grasping force output to overcome strong adhesion forces. Moreover, frictional grasping does not work well at the nanoscale because contact-induced friction forces are often less than the relatively large adhesion forces attributable to the small contact areas that are favorable for nanoobject release.

In order to understand physical interactions during mechanical nanoscale grasping, based on the Hertz [18], JKR [19], DMT [20] and some other extended theories, various contact profiles among a flat surface, sphere and cylinder for different types of fingers and nanoobjects are analyzed. Grasping capabilities of nanogrippers with single and two-finger configurations are discussed and practical designs of the nanogripper are proposed. As an example, we present a prototype of AFM nanomanipulation system, in which two collaborative cantilevers with protruding tips are used to form a dual-tip nanogripper. In our approach, interactions between the nanogripper and the nanoobject during grasping are analyzed and simulated theoretically. We have used the developed nanogripper to pick-and-place nanowires.

2. Contact mechanics of nanoscale grasping

2.1. Problems definition

Modeling and simulation of contact mechanics between the nanoobject, the gripper and a substrate is necessary to provide a theoretical estimation of grasping forces, release adhesion forces and maximum contact stress for reliable pickup and smooth release operations, as well as protecting the gripper and the nanoobject from damage. Research on the following aspects associated with nanoscale grasping should be addressed.

Adhesion force. The effects of adhesion during a nanoscale grasping operation are on friction and interfacial wear as well as a contribution to pickup and release operations, e.g, adhesion forces between a gripper and a nanoobject can be used to counteract substrate adhesion. On the other hand, control and reduction of the adhesion between the gripper and the nanoobject is essential for the release operation.

Nanoscale friction. The empirical da Vinci–Amontons' laws, common knowledge in macroscopic friction as related to the outcome of a collective action of a number of asperities, are no longer suitable for nanoscale contact as it is regarded as a single-asperity contact where the friction is dependent on the contact area [21] and Young's modulus [22] of the contacting interface.

Contact stress. To protect the brittle gripper and the nanoobject from damage, it is essential to predicate the maximum stress at the contact area and maintain it below the contact yield stress. If the adhesion forces, external load, contact area and the stress distribution are known, the contact stress can be accurately estimated.

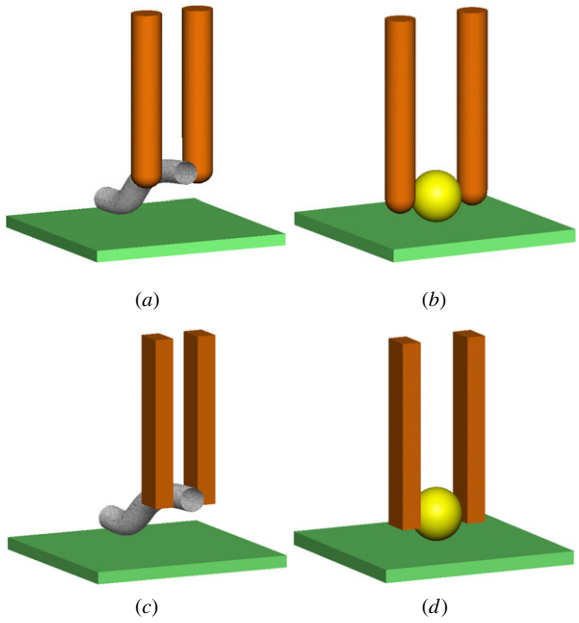

Figure 1. Contact configurations of nanowire/tube and nanoparticle (sphere) grasping with two-finger grippers. In (*a*) and (*c*), the nanowire/tube is grasped by grippers with cylindrical and rectangular fingers, respectively. In (*b*) and (*d*), the nanoparticle is grasped by grippers with cylindrical and rectangular fingers, respectively.

Grasping. To pick up the nanoobject, the grasping force must be greater than the adhesion forces applied on the nanoobject by the substrate. The grasping force may be comprised of adhesion forces, friction forces, or other interactive forces. To obtain an adequate and stable grasping force, some basic problems need to be identified, such as interaction analysis, proper gripper configuration design, and choice of effective grasping strategies and techniques.

Release. To release the nanoobject in its target position, interactive forces in the releasing direction applied from the gripper should be less than the adhesion forces from the substrate. Solutions are needed to reduce the effects of the adhesion forces from the gripper, such as a method to decrease the contact area, surface modifications, and external actions with special manipulation schemes.

2.2. Contact configurations

Figure 1 shows four configurations of nanoscale grasping configurations using two types of two-finger grippers with cylindrical and rectangular fingers. Each configuration uses a nanowire/tube or nanoparticle (sphere). Hence, possible contact states between the gripper and the nanoobject being grasped can be classified as follows.

(i) Contact between two cylinders (C–C), as seen in figure 1(*a*), where the contact is between a nanowire/tube and cylindrical fingers.
(ii) Contact between a cylinder and a sphere (C–S), as seen in figure 1(*b*), where a nanoparticle is grasped by cylindrical fingers.

(iii) Contact between a flat surface and a cylinder (FS–C). Figures 1(*a*) and (*c*) show contacts between a nanowire/tube and the substrate or rectangular fingers.
(iv) Contact between a flat surface and a sphere (FS–S), as seen in figures 1(*b*) and (*d*) where the contact is between a nanoparticle and the substrate or rectangular grippers.

The contacting states depend on the surface profile of the gripper's fingers and the nanoobject with which they are in contact. Contact mechanics of these four states will be discussed in detail in the following parts.

2.3. Mechanics analyses of different contact profiles

2.3.1. Contact mechanics based on the Hertz theory. In a general case, i.e. when two surfaces are brought into contact under a load P, assuming that the contact area is elliptical in shape with semi-axes a and b, the size of the elliptical contact area S can be calculated from [23]

$$S = \pi ab = \pi \left(\frac{3PR_e}{4E^*}\right)^{\frac{2}{3}} [F_1(e)]^2 \tag{1}$$

and the maximum pressure p_0 on the contact area is given by

$$p_0 = \frac{3P}{2\pi ab} = \left(\frac{6PE^{*2}}{\pi^3 R_e^2}\right)^{\frac{1}{3}} [F_1(e)]^{-2}, \tag{2}$$

where R_e is the equivalent radius of the contact area, E^* are the elastic constants of the contact interface, and $F_1(e)$ is deduced from complete elliptic integrals of the argument $e = (1 - \frac{b^2}{a^2})^{\frac{1}{2}}$, $b < a$.

Nanoscale contact can be described with the Hertz model by considering the surface forces in terms of the associated surface energy. As seen in (2), adhesive contact areas can be estimated by adding adhesion forces to the external force P. In addition, the JKR and DMT models, both based on the Hertz model, are widely used to describe totally elastic adhesive spherical contacts. The JKR model is suitable for contacts of soft materials with high surface energies and of spheres with large radii, and the DMT model, in contrast, better suits hard materials with low surface energies and spheres with small radii [24].

2.3.2. Mechanics of C–C contact. As two cylinders (C–C) are brought into contact with arbitrary angle, a gripper with cylindrical fingers (with a radius R_f) is used to grasp cylindrical nanowires (with a radius R_c). Assuming that ψ is the angle by which the cylinder axes are inclined to each other, according to Bradley's approach, the adhesion force between two contacting cylinders can be calculated [25]:

$$F_s = \frac{4\pi R\Delta\gamma}{\sin\psi} \tag{3}$$

where $\Delta\gamma$ is the work of adhesion, $R = \frac{R_f R_c}{R_f + R_c}$. It can be found that the adhesive force between two rigid cylinders is independent of the size of the contact zone. Consequently, from (1) and (3), a contact area between two crossed cylinders can be calculated:

$$S = \pi \left[\frac{3(P + F_s)R_e}{4E^*}\right]^{\frac{2}{3}} [F_1(e)]^2. \tag{4}$$

p_0 can also be deduced from (2) and (3):

$$p_0 = \left[\frac{6(P + F_s)E^{*2}}{\pi^3 R_e^2}\right]^{\frac{1}{3}} [F_1(e)]^{-2}. \tag{5}$$

2.3.3. Mechanics of C–S contact. As a spherical nanoobject (with a radius R_s) and a cylindrical gripper are brought into contact, from (7), if we set $\psi = 90^\circ$ and $R = \frac{R_f R_s}{2R_f + R_s}$, an approximate adhesion force of C–S contact is given by

$$F_s = 4\pi R\Delta\gamma. \tag{6}$$

Similarly, the contact area S and the maximum pressure p_0 can be respectively calculated by substituting (6) into (1) and (2).

2.3.4. Mechanics of FS–C contact. Adhesive contact between a flat surface and a cylinder (FS–C) has been studied with a JKR model [26] to model integrative forces between a flat surface and a cylindrical nanoobject, e.g. nanowires or nanotubes:

$$\frac{P + F_s}{l} = \frac{\pi E^* a^2}{4R} + \sqrt{2\pi E^* a\Delta\gamma} \tag{7}$$

where l is the length of the cylinder, a is the half-width of the contact and the JKR pull-force F_s for line contact is [27]

$$F_s = \tfrac{3}{2} l(4\pi E^* R\Delta\gamma^2)^{\frac{1}{3}}. \tag{8}$$

Thus, from (7) and (8), a half-width a can be calculated and then the contact area $S = 2al$ and $p_0 = \frac{3}{2}\frac{P+F_s}{S}$.

2.3.5. Mechanics of FS–S contact. In the case of a sphere on a flat surface, the contact area S is approximately given by the JKR (for the lower boundary) or DMT (for the higher boundary) contact model. According to the Maugis parameter $\lambda = \delta_0\left(\frac{R}{\Delta\gamma E^{*2}}\right)^{1/3}$ (δ_0 is limiting surface stress) [28],

$$\lambda < 0.1 \Rightarrow \text{DMT}, \qquad S = \pi \left[\frac{R}{K}(P + 2\pi R_s\Delta\gamma)\right]^{\frac{2}{3}} \tag{9}$$

$$\lambda \in (0.1, 5) \Rightarrow \text{Dugdale}, \qquad S = \pi m_0^2 \left(\frac{\alpha + \sqrt{1 + \frac{P}{F_s}}}{1 + \alpha}\right)^{\frac{4}{3}} \tag{10}$$

$$\lambda > 5 \Rightarrow \text{JKR}, \qquad S = \pi \left[\frac{R_s}{K}(P + 3\pi R_s\Delta\gamma + \sqrt{6\pi R_s\Delta\gamma P + (3\pi R_s\Delta\gamma)^2})\right]^{\frac{2}{3}} \tag{11}$$

where $K = \frac{4}{3}\left(\frac{1-\nu_1^2}{E_1} + \frac{1-\nu_2^2}{E_2}\right)^{-1}$ is the reduced elastic modulus for the contact interface, in which ν_1 and ν_2 are the Poisson ratios, and E_1 and E_2 are the Young moduli of each sphere; m_0 can be calculated by

$$m_0 = \left(1.54 + 0.279\frac{2.28\lambda^{\frac{1}{3}} - 1}{2.28\lambda^{\frac{1}{3}} + 1}\right)\left(\frac{\pi\Delta\gamma R_s^2}{K}\right)^{\frac{1}{3}} \tag{12}$$

where α can be calculated from $\lambda = -0.924\ln(1 - 1.02\alpha)$, and F_s for Dugdale theory can be given by

$$F_s = \pi\left(\frac{7}{4} - \frac{1}{4}\frac{4.04\lambda^{\frac{1}{4}} - 1}{4.04\lambda^{\frac{1}{4}} + 1}\right) R_s\Delta\gamma. \tag{13}$$

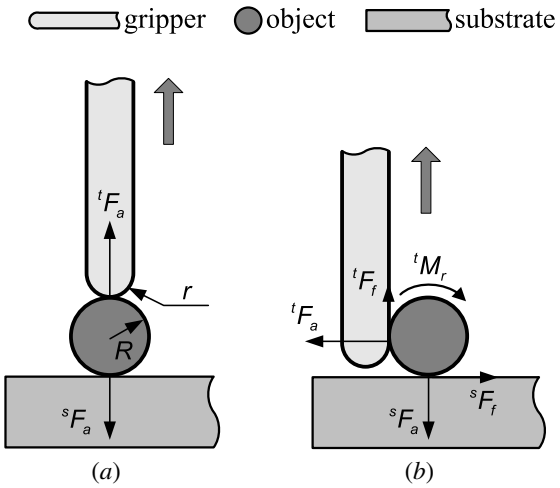

Figure 2. Nanoscale grasping with the single-finger gripper. (*a*) 'Tip grasping' method. (*b*) 'Side grasping' method.

2.4. Friction forces at the contact interface

The well-known Amontons' law shows that a friction force is proportional to a normal force applied on two contacting surfaces with many asperities. However, as the contact area reduces to the nanoscale, the friction with a single asperity contact is more suitably described by [29]

$$F_f = \tau S \tag{14}$$

where τ is a effective friction coefficient, and S is the contact area that is associated with the sum of the external force and the adhesion force. τ is related to the effective shear stress of the contact interface: $\tau \approx 0.0345\,G^*$ [30], where $G^* = \left(\frac{2-\nu_1}{G_1} + \frac{2-\nu_2}{G_2}\right)^{-1}$, ν and G are the Poisson ratio value and shear strength of each of the contacting surfaces, respectively.

3. Nanoscale grasping with different grippers

Grippers with one or two fingers are widely proposed in micro/nano-applications. However, grippers with more than two fingers may meet difficulties in finger mounting within a limit space, and in simultaneously aligning several fingers with nanoscale accuracy, as well as in releasing nanoobject from excessive adhesive contacts. Thus, single- and two-finger grippers are discussed.

3.1. Grasping with the single-finger gripper

Figure 2 shows two grasping schemes with a single-finger gripper, namely 'tip grasping' with fingertip contact and 'side grasping' using the finger side.

3.1.1. 'Tip grasping'. As shown in figure 2(*a*), in order to grasp and release a nanoobject with a single finger, the following inequalities should hold:

$$\begin{cases} {}^tF_a^{\max} > {}^sF_a, & \text{grasp} \\ {}^tF_a < {}^sF_a, & \text{release} \end{cases} \tag{15}$$

where the adhesion forces ^tF_a and ^sF_a, respectively, come from the gripper and the substrate. At present, it is difficult to obtain these inequalities since the contact area of the tip–nanoobject contact is often less than that of the nanoobject–substrate contact.

Grasping at the atomic scale has been demonstrated using the scanning probe microscope (SPM) tip with external energy induced by electric field trapping [31], tunneling current-induced heating or inelastic tunneling vibration [32]. Until recently, nanoscale grasping using a single AFM tip has been achieved with electro-enhanced capillary forces [33]. However, pick-and-place at the nanoscale is still not well resolved with the 'tip grasping' method. Difficulties in this case are weak grasping force outputs while controlling over the applied forces, as well as release accuracy since the single finger has no sufficient geometric limits on the grasping operation.

3.1.2. 'Side grasping'. Figure 2(*b*) shows the 'side grasping' method using the following inequalities:

$$\begin{cases} {}^tF_f^{\max} > {}^sF_a, & \text{grasp} \\ {}^tF_f < {}^sF_a, & \text{release} \end{cases} \tag{16}$$

where ^tF_f is the friction force derived from the adhesion force ^tF_a from the finger side, and ^sF_a is the adhesion force applied on the nanoobject from the substrate.

It is obvious that this method aims to increase ^tF_a through contact with the side rather than contact with the tip. ^tF_a should generally be much larger than ^sF_a to produce enough friction force to satisfy the inequalities. In this case, the release seems more difficult than with the 'tip grasping.' The 'side grasping' scheme is usually used for nanowire/tube grasping in the SEM, which allows many grasp or release attempts using visual feedback. However, 'side grasping' has similar difficulties to those for the 'tip grasping' method, and nanoobject release is to some extent harder.

3.2. Nanoscale grasping with two-finger grippers

Figure 3 shows nanoscale grasping with two-finger grippers. Grippers with parallel- and nonparallel-finger configurations are considered.

3.2.1. Parallel fingers. Figure 3(*a*) shows a gripper that has two parallel fingers with a tip radius of r. To vertically pick up the nanoobject with a radius R, the following inequalities should hold:

$$R > r \qquad \text{and} \qquad {}^tF_f^{\max} > \tfrac{1}{2}{}^sF_a. \tag{17}$$

During the grasping operation, the friction force ^tF_f can be adjusted by increasing or decreasing the repulsive force ^tF_p by driving single or dual fingers. Similarly, for a stable vertical release of the nanoobject, the grasping force can be reduced to generate a certain value of $^tF_f^0$ that makes the nanoobject easily stick on the substrate with the following inequalities:

$${}^tF_f^0 < \tfrac{1}{2}{}^sF_a \qquad \text{and} \qquad {}^tF_f^0 \geqslant {}^tF_f^{\text{ad}} \tag{18}$$

where $^tF_f^{\text{ad}}$ is the adhesive friction force derived from ^tF_a without any external clamping forces.

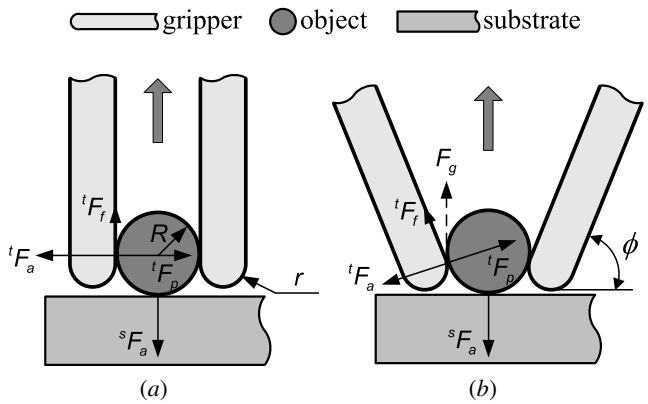

Figure 3. Nanoscale grasping with two-finger grippers. (*a*) The gripper with parallel fingers. (*b*) The nonparallel gripper with a 'V' configuration.

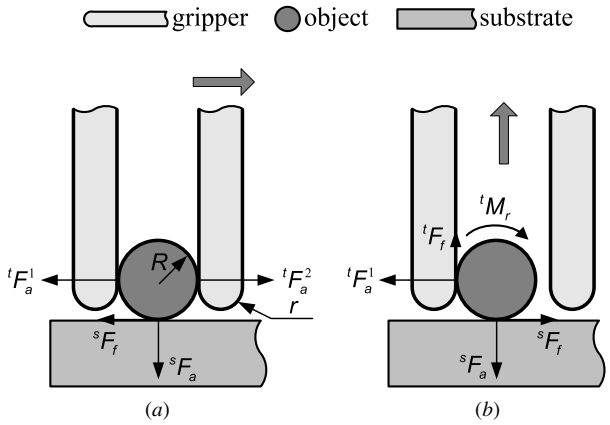

Figure 4. Release operation of the two-finger gripper. (*a*) Horizontally open the gripper by driving the right finger. (*b*) Vertically release the nanoobject.

MEMS grippers have been used to demonstrate vertically aligned carbon nanotube pick-up in the SEM [14]. However, this type of MEMS grippers might meet difficulties when grasping nanotubes attached horizontally to a substrate due to their coarse fingertips, as well as the small gripper–nanotube contact area, which cannot provide a sufficient grasping force (friction forces). This fact is explored in detail in the example of a CNT nanotweezer evaluation given in section 4.

3.2.2. Nonparallel fingers. Fingers with a nonparallel alignment with 'V' configuration shown in figure 3(*b*) are designed to increase the grasping capability. For nonparallel fingers, the following inequalities should hold to successfully pick up the nanoobject:

$$R > r \qquad \text{and} \qquad F_g = \left({}^tF_f^{\max}\cos\phi + {}^tF_p\sin\phi\right) > \tfrac{1}{2}{}^sF_a. \tag{19}$$

Obviously, the tilted angle ϕ makes the grasping stronger as a result of the combined effect of the clamping forces ^tF_p and the friction forces ^tF_f to overcome the adhesion forces ^sF_a.

3.2.3. Release schemes. The release operation of the two-finger gripper is more complicated than the single-finger gripper. Particularly a two-finger gripper with rectangular fingers is used, which produces the comparable adhesion forces ^tF_a and ^sF_a. In contrast, cylindrical fingers may produce smaller adhesion forces, resulting in easier nanoobject release.

As shown in figure 4(*a*), in the first step of the release, the right finger moves to the right to separate from the nanoobject. In this case, the two opposing adhesion forces from the fingers cancel each other out and the friction force ^sF_f is used to hold the nanoobject. When the right finger has been separated from the nanoobject, the gripper moves upward in figure 4(*b*) for the release operation with the following conditions: $^tF_f < {}^sF_a$. Note that in this last step, the nanoobject may roll with a small angle due to ^tM_r derived from ^tF_f. However, apart from the release accuracy, this scheme may be effective for the two-finger gripper release operation.

Table 1. Interfacial contact parameters of materials used in simulation and experiments.

		Silicon	SiO_2	Gold
Surface energy ($J\,m^{-2}$)	γ	1.4	0.16	1.5
Young's modulus (GPa)	E	160	73	79.5
Poisson's ratio	ν	0.17	0.165	0.42

3.3. Grasping capability comparisons of two-finger grippers

3.3.1. Grasping force. To compare grasping forces of the parallel- and nonparallel-finger gripper, an example of nanowire grasping in air with a cylindrical gripper is simulated. The nanowire is horizontally deposited on a substrate and vertical grasping makes an orthogonal contact between the gripper and the nanowire. Suppose that the gripper and the nanowire are made of silicon with a very thin SiO_2 coating and with the same radius of 50 nm. ^tF_f can be estimated by (6), (4) and (14) with mechanics parameters of Si and $\gamma_{SiO_2} = 0.16\ J\,m^{-2}$ described in table 1. For ^tF_a calculation, the work of adhesion $\Delta\gamma$ at the contact interface is calculated by the Dupré equation [34]

$$\Delta\gamma = \gamma_1 + \gamma_2 - \gamma_{12} \tag{20}$$

where γ_1 and γ_2 are, respectively, the surface energies of the contact surface, and γ_{12} is the interface energy. For two solid contact surfaces, $\Delta\gamma = 2\sqrt{\gamma_1\gamma_2}$. The surface energy of the water layer on the contact interface $\gamma_{H_2O} = 0.073\ J\,m^{-2}$.

The simulated grasping force F_g is plotted in figure 5 as a function of the angle ϕ and the clamping force ^tF_p. The result shows that the fingers with a smaller tilted angle tend to produce a greater grasping force. For example, as seen in point A, the parallel gripper, with a clamping force $^tF_p = 2897$ nN, generates $p_0 = 12$ GPa, a yield stress of Si at the nanoscale (12–13 GPa) [29]. In comparison, the nonparallel gripper with a tilted angle of 70° produces eight times more grasping force than the parallel gripper with the same clamping force, as seen in point B. In addition, the grasping force from the parallel gripper is still below the pickup critical force that is normally about several hundreds of nanonewton.

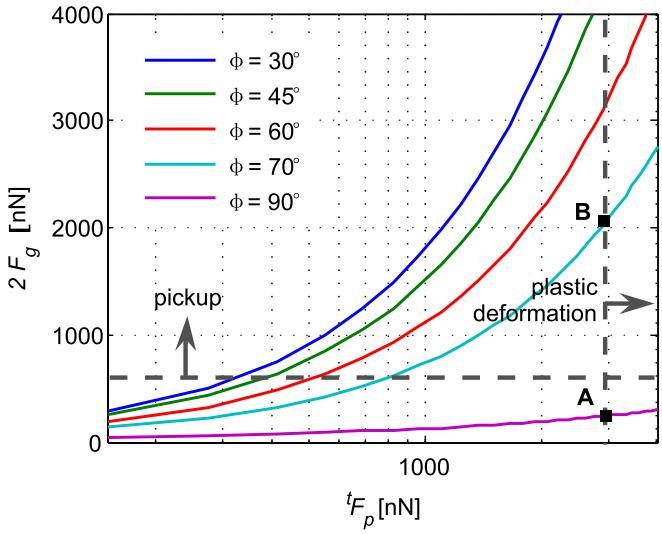

Figure 5. Simulated grasping forces F_g with different clamping angles.

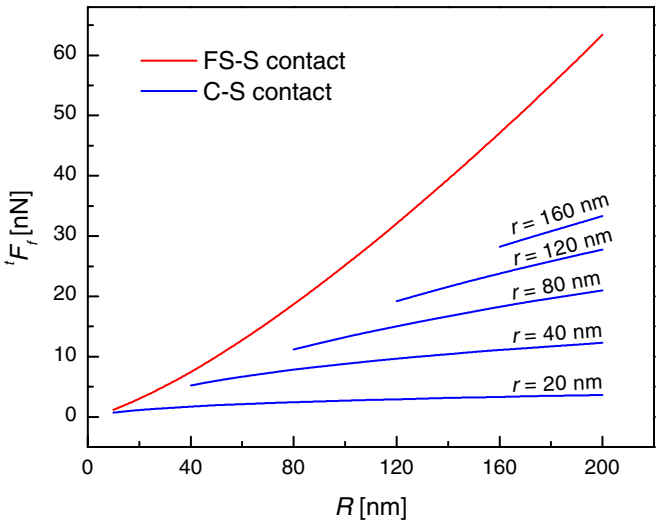

Figure 6. Simulated adhesive friction forces of the rectangular and the cylindrical grippers.

3.3.2. Releasing capabilities. An example of grasping a gold nanoparticle $R = 50$ nm deposited on a Si substrate with a silicon rectangular gripper is presented. We can calculate $^sF_a = {}^tF_a = 243$ nN using (13) ($\lambda = 3.38$) and adhesive friction forces $^sF_f = {}^tF_f = 84$ nN using (14) with interfacial contact parameters of Si and gold described in table 1. The calculated results show that the gold nanoparticle can be successfully released by the rectangular gripper in air. It can be inferred that nanowire release using this scheme is easier than nanoparticle release because of the stronger adhesion force of the nanowire–substrate contact, as calculated from (8).

Theoretical calculation verifies that the rectangular gripper can release the nanoparticle. However, the comparable magnitudes of ^sF_a and ^tF_f introduce uncertainties into the release process, e.g., the nanoparticle skips from the substrate and sticks to the side of the gripper finger even with weak interferences. From (14), values simulated for the adhesive friction forces ^tF_f with the rectangular and cylindrical silicon grippers are plotted in figure 6 as a function of the gold nanoparticle with different radii R. It shows that ^tF_f will be greatly reduced with a cylindrical finger (r in radius) under the same conditions. Moreover, ^tF_f can be further reduced by using thinner cylindrical grippers.

3.4. In summary: fabricating a practical nanogripper

As discussed above, the following items are recommended to fabricate a practical two-finger nanogripper.

(i) Cylindrical fingers (with a circular or elliptical section) with nanoscale radii are proposed for generating low adhesion forces between the grippers and the nanoobject for reliable release.
(ii) Enough clamping stiffness of the gripper is required to produce sufficient clamping forces.
(iii) Nonparallel configuration of the finger alignment is recommended for producing more grasping forces than the parallel alignment.

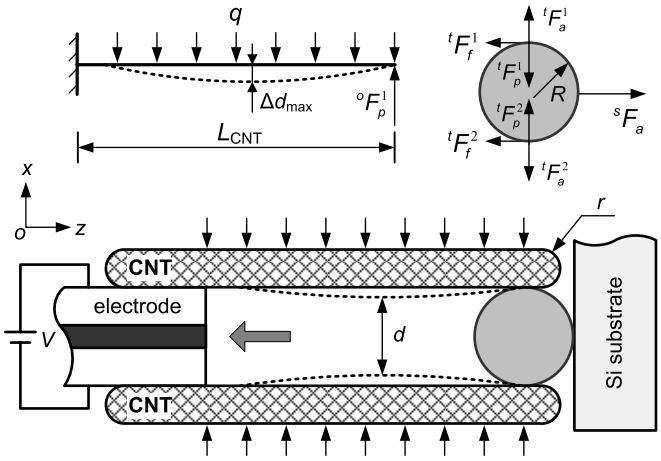

Figure 7. Nanoscale grasping with the CNT nanotweezer.

4. Evaluations of parallel and nonparallel grippers

4.1. Parallel CNT nanotweezer

For further understanding the grasping capability of the parallel-finger gripper, the well-known CNT nanotweezer is taken as an example for grasping a gold nanoparticle deposited on a substrate under ambient environment conditions. For the configuration shown in figure 7, the dimensions of the CNT nanotweezer are $r = 22.5$ nm and $L_{CNT} = 5$ μm, and the parameters of the contact interface are shown in table 1. A natural distance between two CNT fingers is $d_0 = 100$ nm, so a gold nanoparticle radius $R = d_0/2 = 50$ nm is adopted.

To process the hyperstatic electrode–finger–nanoparticle system, as shown in the top inset of figure 7, a force of constraint $^oF_p^1$ is applied on the upper finger that makes the displacement at the end of the CNT finger equal to zero. Assuming that the voltage V applied between the two CNT fingers produces a clamping force q per unit length, $^oF_p^1$ is calculated as

$$^oF_p^1 = \tfrac{3}{8} q L_{CNT}. \quad (21)$$

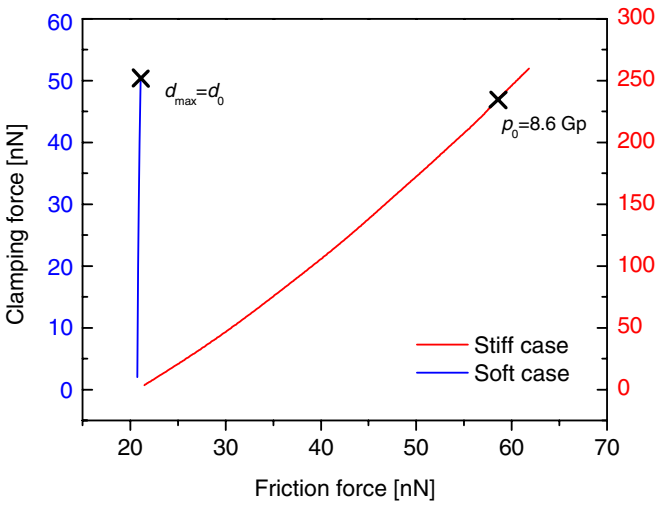

Figure 8. Frictional grasping force of the CNT nanotweezer.

Due to a complicated deflection expression, $\Delta d_{\max}$ is assumed to be obtained at $5L_{\mathrm{CNT}}/8$, which is given by

$$\Delta d_{\max} = \frac{615qL_{\mathrm{CNT}}^4}{32768E_{\mathrm{CNT}}I} \tag{22}$$

where E_{CNT} is Young's modulus of the CNT, I is the moment of inertia of the finger given by

$$I = \frac{\pi r^4}{4}\left[1-\left(\frac{r_{in}}{r}\right)^4\right] = \pi r^4/4 \quad (r \gg r_{in}) \tag{23}$$

where r_{in} and r are, respectively, the internal and outer radii of the CNT finger.

In ambient conditions, ${}^sF_a = 58.4$ nN and the adhesive friction ${}^tF_f = {}^tF_f^1 + {}^tF_f^2 = 20.7$ nN are computed, respectively, by (1) and (14) with $\gamma_{\mathrm{CNT}} = 0.24\,\mathrm{J\,m^{-2}}$, $E_{\mathrm{CNT}} = 1$ TPa and $\nu_{\mathrm{CNT}} = 0.165$. The result shows that the grasping inequality is unsatisfied with only the adhesive friction forces. However, the clamping stiffness of the CNT nanotweezer $k_{\mathrm{CNT}} < 0.01\,\mathrm{N\,m^{-1}}$, which is too soft to produce sufficient grasping forces to pick up the gold nanoparticle, as seen from the blue line in figure 8.

Even assuming $k_{\mathrm{CNT}} \to \infty$ to produce enough clamping forces, e.g., ${}^tF_p^1 = {}^tF_p^2 = 234$ nN for producing a frictional grasping force ${}^tF_f = {}^tF_f^1 + {}^tF_f^2 = 58.4$ nN to suit ${}^sF_a$, as seen from the red line in figure 8, the maximum contact stress $p_0 = 8.6$ GPa exceeds the yield stress of gold at the nanoscale (around 5–6 GPa at 50 nm due to scale effects [35]) and may damage the gold nanoparticle. Again, this example proves that the main difficulty for nanoscale grasping is the fabrication of sharp end-effectors with enough grasping force output.

4.2. Nonparallel dual-tip nanogripper

4.2.1. Nanogripper configuration. Figure 9 shows the setup of a dual-tip nanogripper that is comprised of two individually actuated AFM cantilevers with a protruding tip (see the inset, which are tilted at an angle of 63° between the front side of tip and the cantilever beam). Nanoscale grasping with the proposed nanogripper benefits from its very tiny tip and a nonparallel 'V' configuration, as well as functions of image scanning and force sensing. Detailed descriptions of the system setup and manipulation protocols can be seen in our previous research [36]. In this work, as supplementary contents, mechanics analyses, quantitative calculation of grasping limit improvement and interactive force estimation are detailed based on the contact mechanics research addressed above.

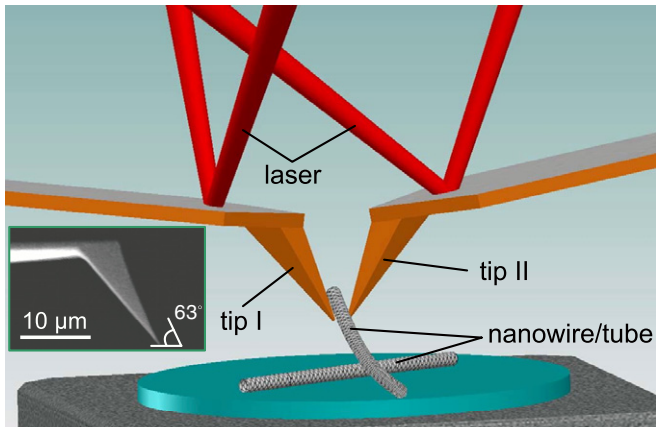

Figure 9. Nonparallel configuration of the dual-tip nanogripper.

4.2.2. Grasping mechanics analysis. Figure 10 shows a schematic diagram of the analysis of the mechanics of a cantilever used as a gripper finger. In experiments, the cantilever's beam length L, beam width w and tip length l are measured under an optical microscope. The beam thickness t is determined using the forced oscillation method [37]. Thus, the normal stiffness k_b^n and the lateral stiffness k_b^l of the cantilever's beam are calculated by

$$k_b^n = \frac{Ewt^3}{4L^3}, \quad k_b^l = \frac{Gwt^3}{3L(l\sin\phi')^2} \tag{24}$$

where E and G are, respectively, the Young and shear modulus of the cantilever, and $\phi' = 60°$ is the tilted angle through the rotation axis of the tip relative to the substrate.

When a force F is applied at the end of the cantilever's tip, it moves with the displacements δ_x, δ_y and δ_z that depend on the stiffness of the cantilever on each axis in the defined frame. As seen in insets (I) and (II) of figure 10, the decoupled displacement on each axis is calculated by

$$\begin{bmatrix}\delta_x\\ \delta_z\end{bmatrix} = \begin{bmatrix}\sin\alpha & \sin\phi' & l\sin\phi'\\ \cos\alpha & \cos\phi' & l\cos\phi'\end{bmatrix}\begin{bmatrix}d_b^{F_x}+d_b^{F_z}\\ d_t^{F_x}+d_t^{F_z}\\ \theta_b^{F_x}+\theta_b^{F_z}\end{bmatrix}, \tag{25}$$

$$\delta_y = F_y\left(\frac{1}{k_b^l}+\frac{1}{k_t}\right) \tag{26}$$

where α is the mounting angle of the cantilever, θ is the angular deflection of the beam d is the deflection of the cantilever's beam and tip (respectively labeled by subscripts b and t, and with superscripts of forces F_x and F_z), and k_t is the stiffness of the cantilever's tip. The calculation of the deflections is detailed in appendix B. The tip close to its very end is

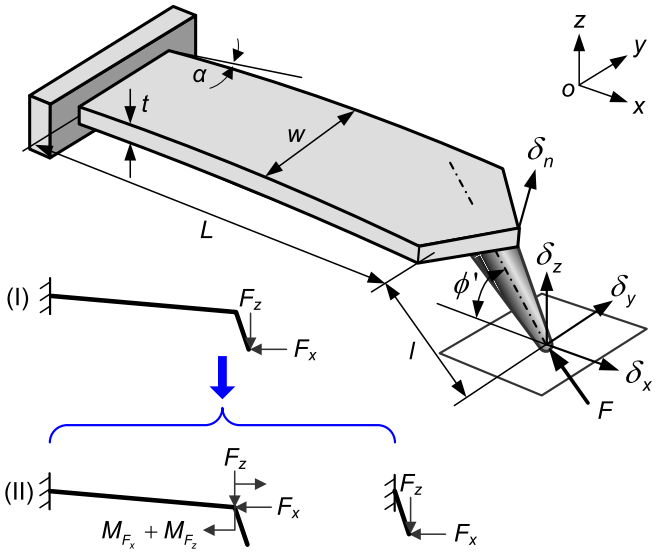

Figure 10. Analysis of the mechanics of the gripper finger (AFM cantilever) during a grasping operation.

assumed to be symmetrical in shape; thus, it has the same stiffness on each axis: $k_t \approx 20\ \mathrm{N\,m^{-1}}$ simulated by the finite element method. From (24), the overall lateral stiffness of the cantilever is about $19\ \mathrm{N\,m^{-1}}$, which makes the tip alignment more stable during the grasping operation.

4.2.3. Grasping capabilities. Figure 11 shows a force simulation for a nanoobject (with a circular section, e.g., nanowires) grasping operation using the proposed nanogripper. Equations can be obtained for a static equilibrium:

$$\begin{cases} F_x = ({}^tF_p \sin\phi - {}^tF_f \cos\phi) \\ F_z = ({}^tF_p \cos\phi + {}^tF_f \sin\phi) = \frac{1}{2}{}^sF_a \end{cases} \tag{27}$$

where $\phi = 68^\circ$ with a mounting angle 5° of the cantilever. ${}^tF_f$ can be calculated by (4) and (14):

$${}^tF_f = \tau\pi \left[\frac{3({}^tF_p + {}^tF_a)R_e}{4E^*}\right]^{\frac{2}{3}} [F_1(e)]^2 \tag{28}$$

where ${}^tF_a = {}^oF_a$, the adhesion force calculated by (3); ${}^tF_p$, the repulsive force from tips, is significant for estimating the maximum stress on the contacting area using (5) to avoid damage to both the nanogripper and the nanoobject.

The normal force F_z and the lateral force F_l applied on the end of the tip can be calculated from the voltage outputs ΔV_n and ΔV_l of optical levers by

$$k_b^n \delta_n = k_b^n \left(d_b^{F_x} + d_b^{F_z}\right) = \Delta V_n S_n, \tag{29}$$

$$F_y = \Delta V_l S_l \tag{30}$$

where δ_n is the normal displacement on the end of the cantilever beam, S_n and S_l are, respectively, the normal and lateral sensitivities of the optical lever. When ΔV_n is detected and ${}^tF_a$ is determined, F_x and F_z can then be calculated by (27).

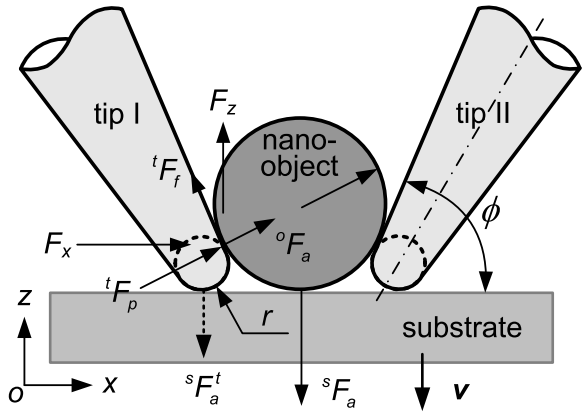

Figure 11. Force diagram using the nonparallel dual-tip nanogripper.

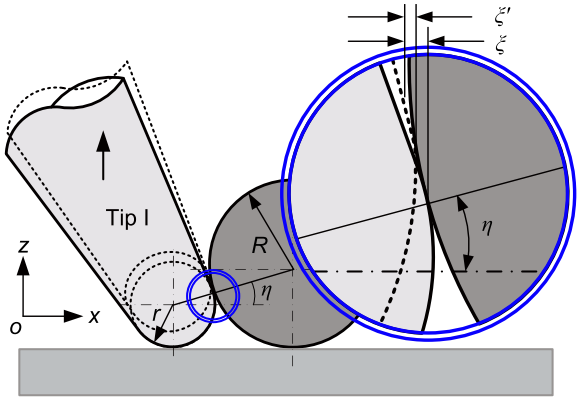

Figure 12. Simulation of the grasping limit on the size of the nanoobject.

As shown in figure 12, for a successful grasping, the angle η as well as the dig-in distance ξ should be positive. Their relation is given by

$$\xi = R(1 - \cos\eta) = R\left[1 - \sqrt{1 - \frac{(R-r)^2}{(R+r)^2}}\right]. \tag{31}$$

During the pickup, the beam and tip deflections cause a smaller ξ', and the grasp is probably lost as ξ is reduced to zero. Thus, the minimum radius of the nanoobject $R_{\min}$ can be estimated by assuming that $\delta_x^{\max} \leqslant \xi$ with known ${}^sF_a$, parameters of the nanogripper and the contacting interface, e.g., Young's modulus, shear modulus and surface energy. $R_{\min}$ can be estimated from the following procedure.

(i) Calculate the adhesion forces ${}^sF_a$ and ${}^tF_a$ with a pre-estimated size limit R_0 of the nanoobject; then calculate the corresponding ${}^tF_a$ and ${}^tF_f$ using (27) and (28).

(ii) When F_x and F_z are calculated by (27), $R_{\min}$ can then be estimated using (25) and (31). Then calculate a new estimation $R_1 = (R_0 + R_{\min})/2$ and repeat the steps with R_1 until the difference between the estimation R_1 and the calculated $R_{\min}$ in successive iterations is less than the predefined $\Delta R = 0.5$ nm.

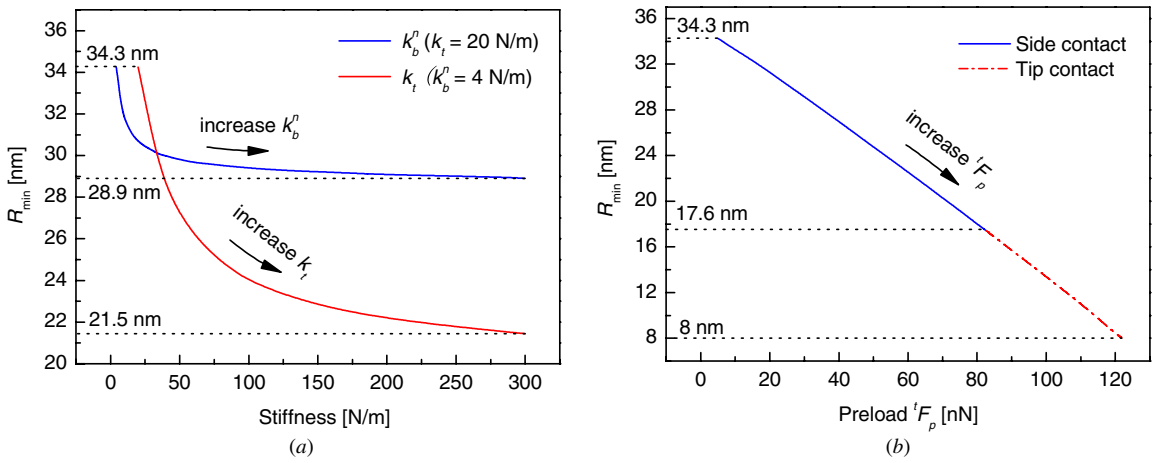

Figure 13. Improving grasping limit by (*a*) increasing stiffness of the cantilever beam k_b^n or tip k_t and (*b*) ^tF_p preloading.

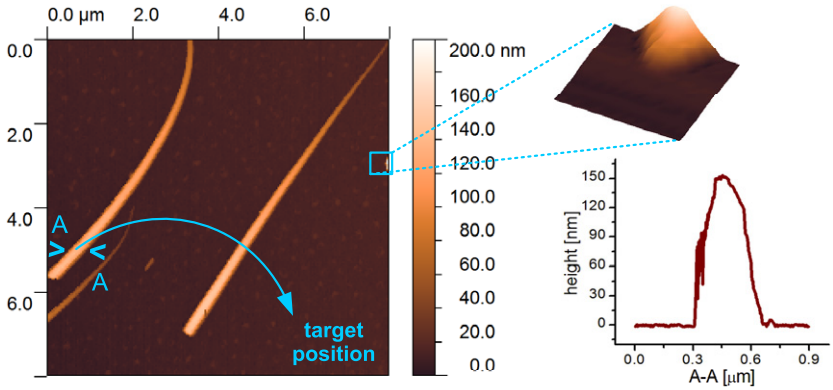

Figure 14. Pre-scanned image of the SiNW. The insets show a 3D topographic image of the tip II and the nanowire height at the location A–A.

Table 2. Dual-tip nanogripper parameters.

k_b^n	k_t	L	l	r	α	^sF_a
4 N m^{-1}	20 N m^{-1}	250 μm	10 μm	8 nm	5°	100 nN

Grasping limit can be improved by increasing k_b^n and k_t. As seen in figure 13(*a*), with parameters described in table 2 (^sF_a is given), the simulated results indicate that a stiffer tip is more effective than a stiffer beam for reducing $R_{\min}$. The former provides a lower limit of 21.5 nm and the later 28.9 nm.

In addition, if a preload of ^tF_p is applied before grasping, the nanogripper will hold the SiNW more tightly with a stronger ^tF_f, thereby significantly reducing $R_{\min}$. As shown in figure 13(*b*), the grasping limit can theoretically equal the radius of the tip apex with a proper preload. However, when the radius of the nanoobject decreases to 17.6 nm, it becomes difficult to grasp because of the contact with the tip apex (sphere–sphere contact). Thus, with this means, $R_{\min}$ reaches the limit of 17.6 nm, while $^tF_p = 83$ nN. However, the preloading involves great risks in damaging the tips as well as the nanoobjects. In this case, the maximum stress p_0 on the contact area should be guaranteed less than the yield stress of the contact.

4.2.4. Silicon nanowires grasping and assembly. In experiments, silicon nanowires (SiNWs) were deposited on a freshly cleaned silicon wafer. A pre-scanned image is shown in figure 14, which includes the topographic image of SiNWs, and the local image of tip II (see the zoomed inset). A grasping location on the left SiNW is marked A–A, where the SiNW has a height of 153 nm. The left SiNW will be transported to the target position where it will be released onto the right SiNW to build a nanocrossbar.

Figure 15 shows an example of contact detection with tip II: seen as icons in the graph, the cantilever is bent upward resulting in positive forces about 5 nN when it snaps in the nanowire. As the tip makes contact with the SiNW, it starts to dig into the root of the SiNW and further movement does not lead to obvious change. During the retraction, the adhesion forces between the tip and the substrate induce a sudden decrease in the bending force to about 48 nN. After the contact breaks with the substrate, the bending force reaches a positive peak before the tip pulls off the nanowire. When the tip digs into the SiNW, the cantilever produces a pre-grasping force $\Delta F_1 = 27$ nN calculated from a voltage difference of about 20 mV and the normal force conversion factor of 1.36 on tip II. The corresponding pre-load on the tip II is estimated as $^tF_p = 26$ nN using (27).

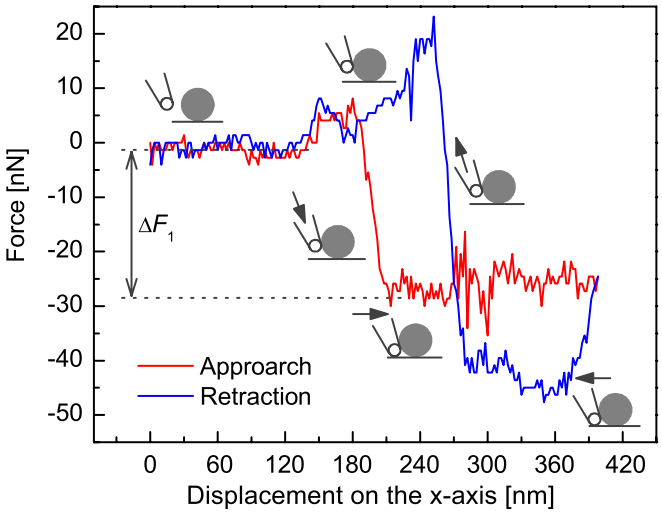

Figure 15. Contact detection by normal force sensing on tip II.

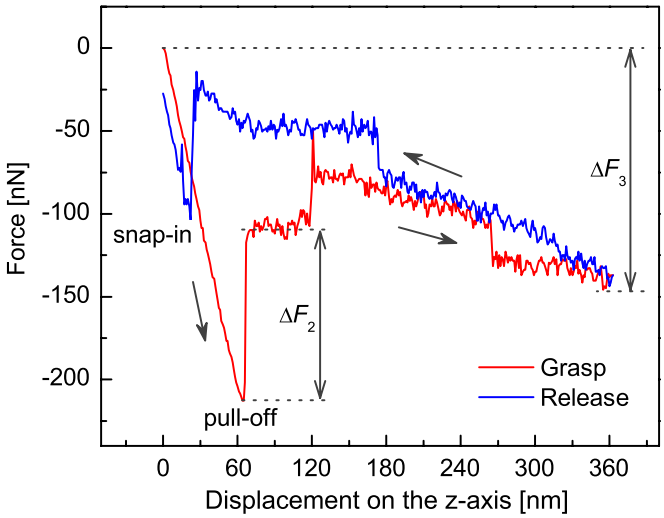

Figure 16. Force detection on one of the tips during the grasping and release operation.

Figure 16 shows the curve of the peeling force spectroscopy on one of the tips during the pick-and-place manipulation of the same SiNW. The curve starts from the contact state between the nanogripper, the SiNW and the substrate. As the nanogripper is moved to pick up the SiNW, the cantilever is bent downward creating negative forces until the cantilever pulls off the substrate with a voltage difference of 75 mV indicating a pull-off force $\Delta F_2 = 103$ nN. As the nanogripper is moved up further, the force magnitude gradually keeps increasing with the SiNW peeling force responses. Retraction leads to a continuous decrease except for a weak fluctuation at 178 nm. Snap-in occurs at 25 nm after a mild force decrease. With even further retraction, the magnitude of the normal force approaches the prior state before grasping.

The maximum peeling force occurs at retraction start, where the voltage is about −105 mV indicating a grasping force of $\Delta F_3 = 144$ nN. At this point, from calculation, ${}^tF_f = 31$ nN that is much smaller than the SiNW–substrate adhesion force, and ${}^tF_p = 218$ nN that generates a maximum contact stress $p_0 = 7.1$ GPa, with $R \approx 19.5$ nm at the contact location of 55 nm from the tip end. Fortunately, this contact stress is still below the yield stress of silicon [29].

The post-manipulation image in figure 17 verifies that the SiNW has been successfully transported and piled on another SiNW, building a nanocrossbar with a maximum height of about 500 nm. During the pick-and-place manipulation, once the SiNW was reliably grasped, the nanogripper moved up 800 nm at a velocity of 80 nm s^{-1}; then the SiNW was transported a distance of 4.05 μm on the *X*-axis at a velocity of 150 nm s^{-1} and 1.95 μm on the *Y*-axis at a velocity of 72 nm s^{-1}.

The SiNWs can be successfully grasped by the proposed nanogripper. However, failure sometimes occurred when grasping positions were located at the middle part of the SiNWs, which jumped from the substrate and then adhered to the nanogripper during the pickup or transportation process. To avoid such failures, grasping locations are strongly recommended at the end of the nanowires/tubes. In addition, the nanowires/tubes should keep in contact with the substrate throughout the pick-and-place process.

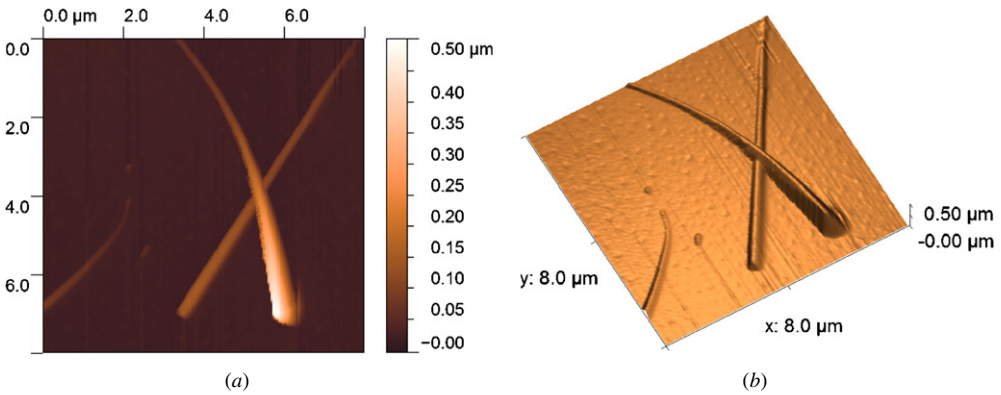

(*a*) (*b*)

Figure 17. Pick-and-place manipulation results for the SiNWs. (*a*) A post-manipulation image verifies that the manipulated SiNW is piled on another SiNW. (*b*) 3D topographic image of the manipulation result.

5. Conclusion

To understand the interactive phenomena between a nanogripper and a nanoobject, contact mechanics were modeled for different contact profiles. Contact modeling made it easy to estimate the interfacial adhesion forces, deduce contact friction forces and contact stress, thereby providing a theoretical analysis for the gripper design. To further improve our understanding, grasping strategies with two-finger grippers were discussed. The analysis shows that the gripper with a nonparallel configuration has better grasping capabilities than the parallel configuration. A homemade nanogripper constructed from two AFM cantilevers with a 'V' configuration was introduced. The grasping capabilities of the proposed nanogripper were analyzed in detail and ways for improving the grasping limitation were presented. Contact mechanics between the tip and the silicon nanowire (the cylinder–cylinder contact configuration) has been analyzed with the modified Hertz model, with which forces applied on the contact area have been estimated, and results show that silicon nanowires can be nondestructively grasped by the proposed dual-tip nanogripper. Subsequently, the nanogripper's capabilities were validated by a successful pick-and-place manipulation of silicon nanowires to build a nanocrossbar. As a result, the theoretical analyses and the experimental results validate the nanoscale grasping schemes and methods with two-finger grippers.

Acknowledgments

This work was supported in part by the ANR (French Research Agency) through the NANOROL Project under ANR grant no PSIROB07-184846. The authors would like to thank Professor Sinan Haliyo and Sébastien Alvo for their valuable discussions.

Appendix A. List of selected symbols

Symbol	*Description*
r	radius of a tip apex
R	radius of a nanoobject being manipulated
S	contact area
p_0	maximum pressure on a contact area
L	cantilever beam length
w	cantilever beam width
t	cantilever beam thickness
l	cantilever tip length
E	Young's modulus
G	shear modulus
E^*	combined elastic modulus
τ	effective friction coefficient
P	external load
F_s	adhesion force
$\Delta\gamma$	work of adhesion
${}^tF_p$	clamping force of a tip
${}^oF_p$	repulsive force on a gripper from a nanoobject
${}^tF_f$	friction force on a nanoobject from a tip
${}^sF_f$	friction force on a nanoobject from a substrate
${}^tF_a$	adhesion force on a nanoobject from a tip
${}^sF_a$	adhesion force on a nanoobject from a substrate
${}^oF_a$	adhesion force on a gripper from a nanoobject
α	cantilever mounting angle
ϕ	tilted angle of a tip through its front edge
ϕ'	tilted angle of a tip through its rotation axis
ψ	inclined angle between axes of contact surfaces
η	effective grasping angle relative to the substrate
ξ	effective grasping distance
k_b^n	normal stiffness of a cantilever's beam
k_t	stiffness of the cantilever's tip
S_n	normal sensitivity of a optical lever
S_l	lateral sensitivity of a optical lever

Appendix B. Deflections on the cantilever

Deflections on the cantilever's beam and tip can be calculated by

$$d_b^{F_x} = \frac{F_x}{k_b^n}\left(\sin\alpha + \frac{3l\sin\phi'}{2L}\right) \tag{B.1}$$

$$d_b^{F_z} = \frac{F_z}{k_b^n}\left(\cos\alpha + \frac{3l\cos\phi'}{2L}\right) \tag{B.2}$$

$$d_t^{F_x} = \frac{F_x\sin\phi'}{k_t} \tag{B.3}$$

$$d_t^{F_z} = \frac{F_z\cos\phi'}{k_t} \tag{B.4}$$

$$\theta_b^{F_x} = \frac{3F_x}{k_b^n L}\left(\frac{\sin\alpha}{2} + \frac{l\sin\phi'}{L}\right) \tag{B.5}$$

$$\theta_b^{F_z} = \frac{3F_z}{k_b^n L}\left(\frac{\cos\alpha}{2} + \frac{l\cos\phi'}{L}\right). \tag{B.6}$$

References

[1] Driesen W, Varidel T, Régnier S and Breguet J M 2005 Micromanipulation by adhesion with two collaborating mobile micro robots *J. Micromech. Microeng.* **15** S259–67
[2] Xie H, Rong W B and Sun L N 2007 A flexible experimental system for complex microassembly under microscale force and vision-based control *Int. J. Optomechatronics* **1** 80–102
[3] Walle B L, Gauthier M and Chaillet N 2008 Principle of a submerged freeze gripper for microassembly *IEEE Trans. Robot.* **24** 897–902
[4] Kim K Y, Liu X Y, Zhang Y and Sun Y 2008 Nanonewton force-controlled manipulation of biological cells using a monolithic MEMS microgripper with two-axis force feedback *J. Micromech. Microeng.* **18** 055013
[5] Neild A P, Oberti S, Beyeler F, Dual J and Nelson B J 2006 A micro-particle positioning technique combining an ultrasonic manipulator and microgripper *J. Micromech. Microeng.* **16** 1562–70
[6] Zhang Y, Chen B K, Liu X Y and Sun Y 2010 Autonomous robotic pick-and-place of micro objects *IEEE Trans. Robot.* **26** 200–7

[7] Xie H and Régnier S 2009 Three-dimensional automated micromanipulation using a nanotip gripper with multi-feedback *J. Micromech. Microeng.* **19** 075009
[8] Menciassi A, Eisinberg A, Izzo I and Dario P 2004 From 'macro' to 'micro' manipulation: models and experiments *IEEE/ASME Trans. Mechatronics* **9** 311–20
[9] Resch R, Lewis D, Meltzer S, Montoya N, Koel B E, Madhukar A, Requicha A A G and Will P 2000 Manipulation of gold nanoparticles in liquid environments using scanning force microscopy *Ultramicroscopy* **82** 135–9
[10] Sitti M 2004 Atomic force microscope probe based controlled pushing for nanotribological characterization *IEEE/ASME Trans. Mechatronics* **9** 343–9
[11] Liu L, Luo Y, Xi N, Wang Y, Zhang J and Li G 2008 Sensor referenced real-time videolization of atomic force microscopy for nanomanipulations *IEEE/ASME T Mechatronics* **13** 76–85
[12] Xie H, Haliyo D S and Reǵnier S 2009 Parallel imaging/manipulation force microscopy *Appl. Phys. Lett.* **94** 153106
[13] Fukuda T, Arai F and Dong L X 2003 Assembly of nanodevices with carbon nanotubes through nanorobotic manipulations *Proc. IEEE* **91** 1803–18
[14] Carlson K, Andersen K N, Eichhorn V, Petersen D H, Mølhave K, Bu I Y Y, Teo K B K, Milne W I, Fatikow S and Bøggild P 2007 A carbon nanofibre scanning probe assembled using an electrothermal microgripper *Nanotechnology* **18** 345501
[15] Sardan O, Eichhorn V, Petersen D H, Fatikow S, Sigmund O and Bøggild P 2008 Rapid prototyping of nanotube-based devices using topology optimized microgrippers *Nanotechnology* **19** 49550
[16] Bosanac L, Aabo T, Bendix P M and Oddershede L B 2008 Efficient optical trapping and visualization of silver nanoparticles *Nano Lett.* **8** 1486–91
[17] Kim P and Lieber C M 1999 Nanotube nanotweezers *Science* **286** 2148–50
[18] Hertz H 1881 On the contact of elastic solids *J. Reine Angew. Math.* **92** 156–71
[19] Johnson K L, Kendall K and Robert A D 1971 Surface energy and the contact of elastic solids *Proc. R. Soc. Lond.* A **324** 301
[20] Derjaguin B V, Muller V M and Toporov Y P 1975 Effect of contact deformations on the adhesion of particles *J. Colloid Interface Sci.* **53** 314
[21] Ritter C, Heyde M, Stegemann B and Rademann K 2005 Contact-area dependence of frictional forces: moving adsorbed antimony nanoparticles *Phys. Rev.* B **71** 085405
[22] Riedo E and Brune H 2003 Young modulus dependence of nanoscopic friction coefficient in hard coatings *Appl. Phys. Lett.* **83** 1986–8
[23] Johnson K L 1985 *Contact Mechanics* (Cambridge: Cambridge University Press)
[24] Schwarz U D 2003 A generalized analytical model for the elastic deformation of an adhesive contact between a sphere and a flat surface *J. Colloid Interface Sci.* **261** 99–106
[25] Wu X F and Dzenis Y A 2007 Adhesive contact in filaments *J. Phys. D: Appl. Phys.* **40** 4276–80
[26] Chaudhurya M K, Weaver T, Hui C Y and Kramer E J 1996 Adhesive contact of cylindrical lens and a flat sheet *J. Appl. Phys.* **80** 30–7
[27] Johnson K L and Greenwood J A 2008 A Maugis analysis of adhesive line contact *J. Phys. D: Appl. Phys.* **41** 155315
[28] Maugis D 1992 Adhesion of spheres: the JKR–DMT transition using a Dugdale model *J. Colloid Interface Sci.* **150** 243–69
[29] Bhushan B 2004 *Springer Handbook of Nanotechnology* (Heidelberg: Springer)
[30] Dedkov G 1999 Friction on the nanoscale: new physical mechanisms *Mater. Lett.* **38** 360–6
[31] Whitman L J, Stroscio J A, Dragoset R A and Cellota R J 1991 Manipulation of adsorbed atoms and creation of new structures on room-temperature surfaces with a scanning tunneling microscope *Science* **251** 1206–10
[32] Avouris P 1995 Manipulation of matter at the atomic and molecular-levels *Acc. Chem. Res.* **28** 95–102
[33] Toset J and Gomila G 2009 Three-dimensional manipulation of gold nanoparticles with electro-enhanced capillary forces *Appl. Phys. Lett.* **96** 043117
[34] Israelachvili J N 1992 *Intermolecular and Surface Forces* (New York: Academic)
[35] Wu B, Heidelberg A and Boland J J 2005 Mechanical properties of ultrahigh-strength gold nanowires *Nature Mater.* **4** 525
[36] Xie H, Haliyo D S and Régnier S 2009 A versatile atomic force microscope for three-dimensional nanomanipulation and nanoassembly *Nanotechnology* **20** 215301
[37] Xie H, Vitard J, Haliyo D S and Régnier S 2008 Enhanced accuracy of force application for AFM nanomanipulation using nonlinear calibration of optical levers *IEEE Sens. J.* **8** 1478–85